Influence of oxygen deficiency on the out-of-plane tilt of epitaxial Y_2O_3 films on Ni–5%W tapes

C. Cantoni,[a] E.D. Specht, and A. Goyal[b]
Oak Ridge National Laboratory, Oak Ridge, Tennessee 37831

X. Li and M. Rupich
American Superconductor Corporation, Westborough, Massachusetts 01581

(Received 12 August 2008; accepted 10 November 2008)

We analyzed the crystallographic *c*-axis tilt of (001) Y_2O_3 films grown on biaxially textured Ni–5%W tapes under different oxygen flux conditions. Results show that different tilting mechanisms were effective in films with different oxygen stoichiometry. Moreover, the structure of the film/substrate interface investigated by transmission electron microscopy, and the residual strain of the film investigated by x-ray diffraction were also dependent on the film oxygen content. Although the oxygen stoichiometric Y_2O_3 sample exhibited a coherent film/substrate interface and the sharpest out-of-plane texture, the films grown under reduced oxygen pressure exhibited a smaller overall *c*-axis tilt due to formation of interface dislocations and regions in which the film oxygen vacancies ordered to form a lattice superstructure.

I. INTRODUCTION

Oxygen deficiency and oxygen vacancies can greatly affect the structural, electronic, and mechanical properties of metal oxides, whether they are used in metal-oxide semiconductor heterostructures, optical applications, corrosion protection, or as buffer layers in high-temperature superconducting (HTS) tapes. One of the key consequences of oxygen substoichiometry for oxide buffer layers in HTS tapes is increased oxygen and metal ion diffusivity, which weakens the functionality of buffers as diffusion barriers.[1] In this work, we explore how oxygen deficiency during the buffer (seed) layer deposition also affects the epitaxial relationship between the oxide film and substrate, the mosaic spread of the film *c* axis, and the residual strain of the film. These variables are of great importance because they determine the texture of subsequent buffer layers and superconducting film, which in turn is strongly related to the superconducting critical current density (J_c) of the HTS tape.[2]

II. EXPERIMENTAL RESULTS

The system investigated here is a biaxially textured {100}⟨100⟩ Ni–5%W alloy substrate tape on which a 75-nm-thick Y_2O_3 film is grown by reactive sputtering from an yttrium metal target. The deposition takes place in a continuous fashion, as the substrate tape is transported into the deposition chamber at one extremity and exits the chamber out the other extremity by means of a reel-to-reel setup. This deposition technique was perfected over the past few years by American Superconducting Corporation (AMSC) and is routinely used to fabricate highly textured HTS tapes with structural and superconducting properties comparable or superior to those found in small tapes fabricated by stationary deposition methods. Details of the deposition process and superconducting properties of the tape are reported elsewhere.[1] The average grain size of the metal substrate is about 50 μm. The out-of-plane and in-plane texture of the substrate results in full width half-maximum (FWHM) values of 6° and 7° for the x-ray diffraction (XRD) ω-scan of the (002) peak and the ϕ-scan of the (111) peak, respectively (Table I).

When the Y_2O_3 seed layer deposition takes place under optimal oxygen flux, the Y_2O_3 film displays a greatly improved out-of-plane texture as compared to the substrate texture. The FWHM for the Y_2O_3 (004) ω-scan becomes more than 3° smaller than the substrate's FWHM for a scan performed in the rolling direction ($\phi = 0$), and nearly 7° smaller than the substrate's FWHM along the transverse direction ($\phi = 90°$). Optimally grown samples show $\Delta\omega = 2.8°$; $\Delta\phi = 4.8°$ for Y_2O_3 and $\Delta\omega = 2.4°$; $\Delta\phi = 5.1°$ for the superconductor. Despite the fact that this mosaic spread exceeds that found in commercial single crystals, the J_c of these tapes, which ranges between 4.8 and 5.0 MA/cm^2 at 77 K

[a]Address all correspondence to this author.
e-mail: cantonic@ornl.gov
[b]This author was an editor of this journal during the review and decision stage. For the *JMR* policy on review and publication of manuscripts authored by editors, please refer to http://www.mrs.org/jmr_policy
DOI: 10.1557/JMR.2009.0065

 © 2009 Materials Research Society

in zero applied field, approaches the highest values reported for single crystal substrates.

On the other hand, nonadequate oxygen supply during deposition results in Y_2O_3 films that show little or no improvement in their texture as compared to the substrate texture. Figure 1 shows the different rocking curves of the Y_2O_3 (004) peak obtained for a set of three samples discussed in this work. To explain the results we need to understand first how sharpening of the out-of-plane texture can occur during epitaxial deposition of the Y_2O_3 film on the NiW substrate, and second, why the oxygen content of the film affects the texture improvement mechanism.

TABLE I. Summary of acquired and calculated XRD data on samples S1, S2, and S3.

Texture	S1	S2	S3
	FWHM (°)	FWHM (°)	FWHM (°)
Y_2O_3(004), $\phi = 90°$, axis is TD	3.00	6.72	6.42
Y_2O_3(004), $\phi = 0°$, axis is RD	2.83	4.19	4.19
Ni(002), $\phi = 0°$, axis is RD	6.27	5.88	6.12
Ni(002), $\phi = 90°$, axis is TD	9.92	10.15	10.13
Ni(111) $\phi = 45°$	7.43	7.28	7.07
Ni(100) in-plane	4.56	4.31	3.87
Y_2O_3(222), $\phi = 0°$	5.79	6.90	7.10
Y_2O_3(222), $\phi = 90°$	5.71	5.95	6.00
Y_2O_3(222), $\phi = 180°$	5.98	6.94	6.86
Y_2O_3(222), $\phi = 270°$	5.76	5.62	6.08
Y_2O_3(100) in-plane	5.43	5.00	5.28
Lattice parameters	S1	S2	S3
Y_2O_3 in-plane lattice parameter a (Å)	10.569	10.579	10.593
Y_2O_3 out-of-plane lattice parameter c (Å)	10.660	10.635	10.621
Average lattice parameter (Å)	10.599	10.598	10.602
Tetragonal distortion $c/a - 1$	0.009	0.005	0.003

Peak FWHM values are found by Gaussian fits to rocking curves and phi scans. In-plane widths are calculated from measured widths as described in Ref. 16. Y_2O_3 lattice parameters are calculated algebraically from the averages of four {622} and four {226} Bragg angles, using the {311} and {113} Bragg angles from a Si(100) wafer (a_0 = 5.4308) for calibration.

RD, rolling direction; TD, transverse direction.

III. MECHANISMS OF TILTED EPITAXY

Changes in the out-of-plane texture of the Y_2O_3 seed can be explained on the basis of crystallographic tilting of epitaxial films, which is a phenomenon known since the beginning of semiconductor heteroepitaxy,[3–5] although its microstructural origins remain poorly understood, especially for large-misfit systems such as ours. The origin of such tilt is attributed to two general types of microstructural mechanisms: step-mismatch mechanisms, and biased dislocation mechanisms. The first mechanism is active on vicinal surfaces for conditions of high surface mobility and at earlier stages of deposition, when the growth is pseudomorphic and strain energy accumulates in the film. In this system, as proposed originally by Nagai,[4] the lattice spacing of the film in the growth direction relaxes from the value d_s (lattice spacing of the substrate) to the film value d_f over the length of a step terrace, introducing a tilt given by

$$\Delta\psi = \tan^{-1}\left(\frac{d_s - d_f}{d_s}\tan\psi\right) \quad ,$$

where ψ is the miscut or vicinal angle. In this model the tilt will be away from the surface normal in the case $d_f > d_s$ and toward the surface normal if $d_f < d_s$. A schematic of this mechanism is illustrated in Fig. 2(a). With layer spacings $d_s(002)$ = 1.76 Å for Ni and $d_f(008)$ = 1.32 Å for Y_2O_3, a sharpening of $\Delta\psi \approx 0.25°$ ψ is predicted for small ψ.

At some critical thickness, misfit dislocations are introduced to relieve the mismatch strain. At this point, the second type of crystallographic tilt mechanism is activated if particular types of dislocations with a net out-of-plane component of the Burgers vector are preferentially inserted. Misfit dislocations with a component $b_\perp$ of the Burgers vector normal to the interface can in fact induce tilting, as shown in the schematic of Fig. 2(b). This dislocation-mediated tilting mechanism can occur after a first stage of strained epitaxial growth or immediately after nucleation in large misfit systems for which layer-by-layer growth does not take place. As shown by

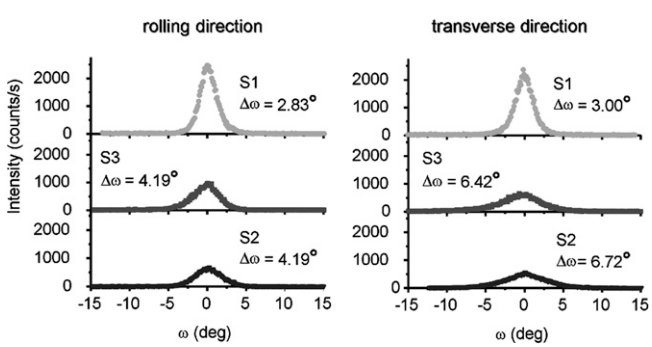

FIG. 1. Rocking curves of the (004) Y_2O_3 peak for the samples discussed in the text. The curves were acquired mounting the samples with $\phi = 0°$ (rolling direction) and $\phi = 90°$ (transverse direction).

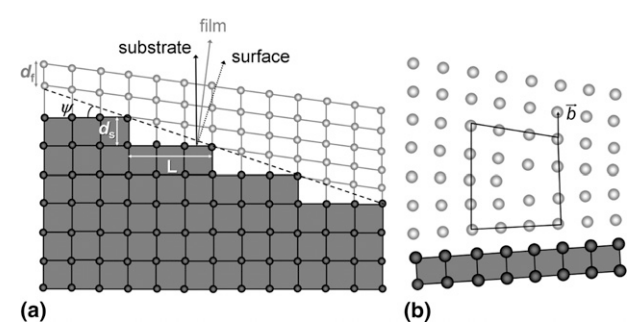

FIG. 2. Schematic of the two crystallographic tilting mechanisms discussed in the text: (a) step mismatch mechanism and (b) biased dislocations mechanism.

Olsen and Smith,[5] if the linear density of dislocations is sufficient to relieve the misfit $f = (d_f - d_s)/d_s$, the film tilt will be $\Delta\psi = f \cdot b_\perp / b_{//}$, where $b_{//}$ is the component of the Burgers vector parallel to the plane of the film. The bias in the distribution of such dislocations (which determine the direction of tilt) can be provided, for example, by the direction of the substrate's step ledges. The biased dislocation mechanism is also known to allow for larger tilts than the step-matching mechanism.

For the crystallographic tilt to be effective in sharpening the film out-of-plane texture, regardless of the active tilting mechanism, the Y_2O_3 film regions growing on each substrate grain need to tilt all toward the same direction: that of the sample's surface normal. In this way the Y_2O_3 (001) poles from each substrate's grain will shift apart from the corresponding substrate (001) poles and converge toward a common center, reducing the film mosaic spread. The larger the Y_2O_3 tilt toward the surface normal for each substrate grain, the sharper the resulting overall out-of-plane texture in the Y_2O_3 film.

In cases in which the Nagai mechanism provides the main contribution to the tilt (coherent interface), the strain induced in the film by pseudomorphic growth on the vicinal surface of each substrate grain will automatically provide a common tilt toward the surface normal, if the film interplane spacing is smaller than that of the substrate. For systems with a large lattice mismatch, coherent growth might not continue for long or take place at all, and misfit dislocations appear in the nucleation stage. In this case (incoherent interface), out-of-plane texture sharpening will occur only if dislocations with a component of the Burgers vector normal to the interface form in the growing film, and their biased distribution is such to generate a tilt toward the surface normal for film regions within each substrate's grain. In particular, Ayers et al.[6] have shown that the unequal distribution of certain misfit dislocations induced by the substrate miscut generates tilts toward the surface normal when $d_f > d_s$, opposite to the tilt direction in pseudomorphic systems.

Budai et al.[7] have found that the sharpening of the out-of-plane texture of CeO_2 films on biaxially textured $\{100\}\langle 100\rangle$ Ni agrees qualitatively with the Nagai tilt mechanism, which predicts shifting of the CeO_2 (001) poles toward the surface normal because d_f for CeO_2 is 1.36 Å, smaller than d_s for Ni (1.76 Å). However, step matching during pseudomorphic growth is not the only tilting mechanism observed for films on biaxially textured Ni or Ni-alloy tapes. It was found that TiN films (d_f = 2.12 Å; $d_f > d_s$) show tilts toward the surface normal as large as 10°, consistently larger than those observed in CeO_2.[8] As shown by reflection high-energy electron diffraction (RHEED) and cross-section transmission electron microscopy (TEM), the growth of TiN on Ni and Ni-alloys is not pseudomorphic and step matching does not occur. Instead, dislocations form readily during film nucleation and growth, and a strong bias in the distribution of dislocation with Burgers vector normal to the interface is responsible for the large tilts observed.

IV. RESULTS AND DISCUSSION

To investigate the mechanism responsible for tilting in Y_2O_3 films on Ni–W, we selected three Y_2O_3/Ni–W samples grown with optimal oxygen partial pressure (S1), slight oxygen deficiency (S2), and severe oxygen deficiency (S3), respectively. The oxygen flow at the substrate during film growth was the only deposition parameter varied in this experiment. The structure of the samples was analyzed by XRD using a Rigaku RU300 Cu rotating-anode source equipped with a curved graphite monochromator and a Huber four-circle diffractometer and by high resolution TEM using a Philips CM200 microscope equipped with field emission gun and operating at 200 KV. Because the different elastic properties and ion milling rates of Y_2O_3 and Ni–W hinder conventional TEM sample thinning, TEM samples were prepared by focused ion beam (FIB) techniques commercially available.

Table I shows a summary of the XRD measurements performed on film and corresponding substrate regions encompassing a statistical number of grains by using an oscillating sample holder, which allows an effective beam scanning over an area of a 2 mm × 2 mm incident beam. We noticed that while the substrate's texture is nominally the same for all samples, substantial sharpening of the out-of-plane texture takes place in the Y_2O_3 grown at optimal oxygen partial pressure. The residual compressive strain in the film is the largest for the optimally oxygenated sample and decreases with oxygen deficiency.

Figure 3 shows the diffraction pattern of the Y_2O_3/Ni–W sample with optimal oxygen composition on a single Ni–W grain and a low magnification high-resolution TEM (HRTEM) image of the interface. The image shows that the interface is atomically sharp and essentially planar with some steps present. The diffraction pattern shows that Y_2O_3 grew, as expected, with an in-plane 45° rotation with respect to the Ni cell, i.e., Y_2O_3 (001) is parallel to Ni (001) and Y_2O_3 (110) is parallel to Ni (100). However, a closer look at the Ni (200) and Y_2O_3 (440) diffraction spots show that Y_2O_3 (110) is not strictly parallel to Ni (100) and the two directions form, in fact, an angle of ~3°. The HRTEM image of the Y_2O_3/Ni–W interface (Fig. 4) gives more insight on the nature of this tilt. In this image, the Y_2O_3 fringes are clearly visible, although the quality of the sample does not allow to clearly resolve the Ni fringes. Nevertheless, it is easy to see that the interface is coherent, and the

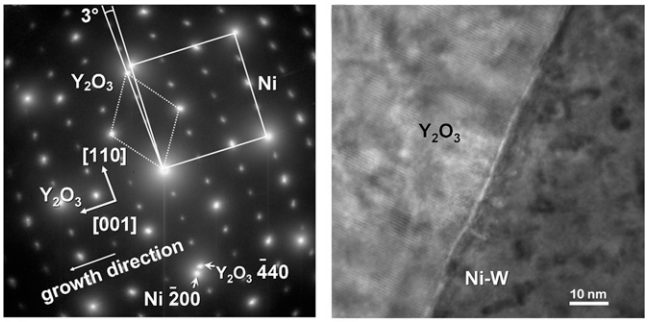

(a) (b)

FIG. 3. TEM data for sample S1. (a) Selective area diffraction pattern showing reflections from the Ni–W substrate and the Y_2O_3 film. A tilt of 3° between substrate and film axis is shown. (b) Low-magnification HRTEM image showing planar substrate/film interface.

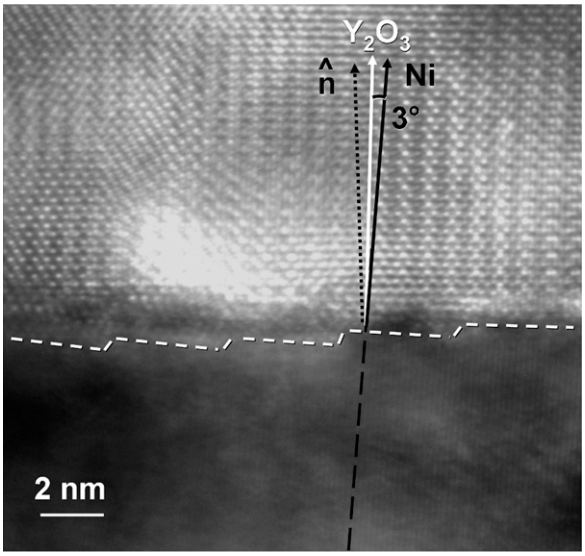

FIG. 4. HRTEM image of the interface region in sample S1. The arrows indicate directions for the surface normal, the substrate *c* axis, and the film *c* axis. The dotted line outlines the direction of the substrate's step ledges.

Ni *c* axis and the Y_2O_3 *c* axis are not parallel but form an angle of ~3°. Moreover, given the orientation of the vicinal steps indicated in the figure, we conclude that the Y_2O_3 *c*-axis tilts toward the surface normal, as verified by the XRD measurements. The TEM data strongly suggest that the Nagai step-matching mechanism is responsible for the film tilt. Therefore, in this case the Y_2O_3 film on Ni–W behaves like the optimal CeO_2 films on Ni of Ref. 7. This is not surprising given the close similarity between the crystal structure of Y_2O_3 and CeO_2 and their similar lattice spacing ($a/2$ = 5.30 Å for Y_2O_3; a = 5.41 Å for CeO_2). As in CeO_2/Ni, the tilt observed here is larger than what can be calculated using Eq. (1). Figure 4 suggests a step terrace of 4–5 nm, which corresponds to a miscut angle of at most 4.5°. If the step-matching mechanism were the only active tilt mechanism, it would produce a tilt in the Y_2O_3 of only 1°. TEM images suggest that a few misfit dislocations are present above a critical thickness of 10–15 nm and that some of these dislocations exhibit an out-of-plane component of the Burgers vector that could explain the larger tilt observed. However, higher quality TEM samples are necessary to further investigate this point. The relatively high strain observed for sample S1 (Table I) is consistent with the observation of few (if any) misfit dislocations.

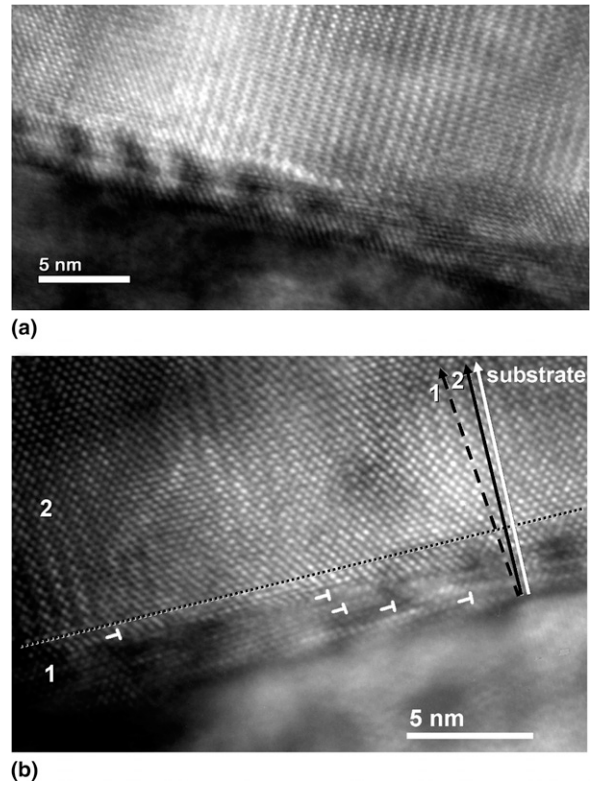

FIG. 5. HRTEM images of the interface between substrate and Y_2O_3 film in sample S2. (a) The dark periodic contrast is associated with strain and dislocations in the Y_2O_3 nucleation layer. The nucleation layer (1) shows a different *c*-axis tilt than the remaining film (2). (b) The arrows represent the two *c*-axis directions for film (1) and film (2), and the substrate <001> direction.

Figure 5 shows two HRTEM images of the interface in sample S2 with intermediate oxygen deficiency. In this case the film tilt in the diffraction pattern is hardly visible, and in agreement with the more modest out-plane-texture improvement measured by XRD, which amounts to 1.7° in the rolling direction and 3.4° in the transverse direction. The HRTEM images show the presence of dislocations in the Y_2O_3 film at the nucleation stage. More precisely, we observed an initial layer with a critical thickness of about 2–3 nm above which the Y_2O_3 fringe contrast changes abruptly through introduction of dislocations. This suggests that film growth proceeded through two different mechanisms. Initially the film nucleated exhibiting a large tilt from the substrate's planes attributable to step-matching strained epitaxy just

as in the optimally processed sample. However, this type of growth mechanism did not continue throughout the thickness and was limited to a very thin layer of ~1 nm, after which unbalanced dislocations having a component of the Burgers vector normal to the surface formed, causing the remaining film to tilt back away from the surface normal and toward the substrate's *c* axis. This is illustrated by the arrows in Fig. 5(b) indicating the [001] vectors of substrate and film and some of the tilt-producing dislocations. As a result, the majority of the Y_2O_3 film shows no dramatic tilt angle between the Ni–W c axis and Y_2O_3 *c* axis. Consequently, the overall Y_2O_3 film grown over multiple Ni–W grains exhibits little improvement in the macroscopic out-of-plane texture as compared to that of the substrate.

As mentioned previously, dislocations with a component of ***b*** normal to the growth plane are expected to show a bias that results in film tilts away from the surface normal in systems with $d_f < d_s$. However, it is not clear why such dislocations arise in this case. Although the CeO_2 crystal cell expands when oxygen deficient and contracts with oxygen uptake from the environment,[9,10] early studies have shown that the yttria lattice cell does not vary in dimensions even when the oxide is greatly reduced.[11–13] Therefore, we cannot attribute the nucleation of dislocations to an increased lattice mismatch between the Y_2O_3 processed in low O_2 pressure and the Ni–W as an analogy with the response of CeO_2 to oxygen substoichiometry would suggest. More likely, the introduction of oxygen vacancies in the growing film is associated with a decrease in the self-energy of this dislocation type in oxygen deficient yttria, which favors nucleation. The introduction of dislocations at the Y_2O_3/Ni–W interface might also be responsible for a reduction in the residual strain of this film as compared to the film grown in optimal oxygen partial pressure. The tetragonal distortion for Y_2O_3 in sample S2 was $c/a - 1 = 0.005$ versus a value of 0.009 for sample S1 (see Table I).

We now analyze the effects of oxygen deficiency on sample S3. As shown in Table I, sample S3 has a texture similar to sample S2. The Y_2O_3 film shows a sharpening in the out-of-plane but not as dramatic as in sample S1. The improvement for $\Delta\omega$ in the Y_2O_3 film compared to the Ni–W substrate is 1.9° in the rolling direction and 3.7° in the transverse direction. However, the TEM data show a completely different film structure than that observed in samples S2 and S1. The Y_2O_3 lattice exhibits a superstructure in several regions starting at the interface. Figure 6(a) shows one of such regions where the superstructure creates characteristic dark/light fringes parallel to the interface (perpendicular to the Y_2O_3 *c* axis). Figure 6(b) shows by comparison a "normal" interface region where no such fringes are observed. The insets in Figs. 6(a) and 6(b) show the digital diffraction pattern of the two HRTEM images. We noticed that the digital

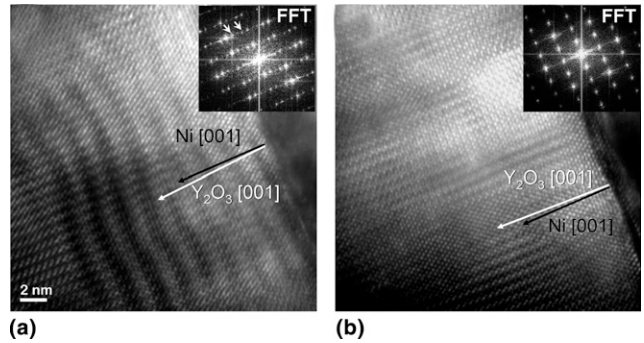

FIG. 6. HRTEM images and corresponding fast Fourier transforms (FFT) of two different interface regions in sample S3. (a) Light and dark contrast fringes perpendicular to the Y_2O_3 *c* axis represent a superstructure formed by ordering of oxygen vacancies. The superstructure gives extra reflections in the FFT that are not normally seen in yttria diffraction patterns. (b) In addition to the superstructure regions, the sample shows alternating normal Y_2O_3 regions.

diffraction pattern in Fig. 6(a) shows additional reflections, which are attributed to the superstructure region and are absent in the normal region of Fig. 6(b). The same additional reflections are also visible in the Y_2O_3 SAD pattern (not shown), which samples a film area containing normal and superstructure regions.

The existence of a similar superstructure in oxygen deficient Y_2O_3 films was reported previously by others and attributed to ordering of oxygen vacancies.[14,15] We surmise that when the oxygen partial pressure during deposition is low enough to cause formation of large numbers of oxygen vacancies in the growing film, these tend to cluster and order into a superstructure, creating regions in which the film is highly oxygen deficient next to stoichiometric Y_2O_3 regions.

A close comparison of the Y_2O_3 lattice fringes within the two regions reveal that the respective [001] vectors are not parallel. Although the Y_2O_3 [001] in the normal regions points toward the surface normal, the [001] of the superstructure regions points in the opposite direction and therefore lessens the sharpening effect associated with the strained epitaxial growth of optimally doped Y_2O_3. The reason for the different tilt direction of the superstructure regions is not clear, but we suspect that this might be related to changes in the number of oxygen atoms that are coordinated to each Y atom, and the greater spread of bond lengths between near neighbor atoms observed in reduced yttria.[12,13] We recall that in Y_2O_3, the (00l) lattice planes consist of alternating O-planes and Y-planes spaced 1.33 Å apart. This is the lattice spacing that will match the Ni–W inter-plane lattice spacing of 1.76 Å in the <001> direction at the substrate's step ledges. Vacancies in the O-planes and a spread in the Y–O bond lengths associated with the superstructure might change the nature of the bonds between Ni atoms and yttria atoms at the step ledges, thus

modifying the crystallographic film tilt. A change in number of next neighbors and bond lengths might be related in general to a lower epitaxial strain in the superstructure regions, which would also account for the smaller tetragonal distortion measured for this film as compared to samples S1 (Table I). Alternatively, the epitaxial strain may be relieved by misfit dislocations. Although dislocations are not apparent at the film-substrate interface, it is unclear how abundantly they occur as the film thickness increases above a critical value of ~10–15 nm.

Finally, we exclude the possibility that chemisorption of oxygen or other species on the Ni–W surface before film deposition might play a role in determining the tilts observed in these samples. In all cases the Ni–W substrates were subjected to the same sulfur treatment designed to ensure formation of a c (2×2) S superstructure throughout the metal surface. The S termination was found previously to enable the Y_2O_3 epitaxial growth,[17,18] and is known to be stable at all oxygen pressures used for buffer layer deposition on Ni–W, and in severe reducing environments as well.

In summary, we have shown that low oxygen partial pressure during Y_2O_3 growth on Ni–W affects not only the film oxygen content but also the film tilt with respect to the substrate, film microstructure, and film nucleation mechanism. The oxygen stoichiometric Y_2O_3 sample exhibited a coherent film/substrate interface and strain-mediated crystallographic tilt of the type described by Nagai et al.[4] However, in the films grown under reduced oxygen pressure the effects of this tilt mechanism were greatly diminished due to formation of interface dislocations or regions in which the film oxygen vacancies ordered to form a lattice superstructure.

ACKNOWLEDGMENT

Research was sponsored by the United States Department of Energy, Office of Electricity Delivery and Energy Reliability–Superconductivity Program, under Contract DE-AC05-00OR22725 with UT-Battelle, LLC managing contractor for Oak Ridge National Laboratory.

REFERENCES

1. A. Goyal, M. Paranthaman, and U. Schoop: The RABiTS approach: Using rolling-assisted biaxially textured substrates for high-performance YBCO superconductors. *MRS Bull.* **29**(8), 552 (2004).
2. E.D. Specht, F.A. List, D.F. Lee, K.L. More, A. Goyal, W.B. Robbins, and D. O'Neill: Uniform texture in meter-long $YBa_2Cu_3O_7$ tape. *Physica C* **382,** 342 (2002).
3. F. Riesz: Crystallographic tilting in high-misfit (100) semiconductor heteroepitaxial systems. *J. Vac. Sci. Technol., A* **14,** 425 (1996).
4. H. Nagai: Structure of vapor-deposited $Ga_xIn_{1-x}As$ crystals. *J. Appl. Phys.* **45,** 3789 (1974).
5. G.H. Olsen and R.T. Smith: Misorientation and tetragonal distortion in heteroepitaxial vapor-grown III-V Structures. *Phys. Status Solidi A* **31,** 739 (1975).
6. J.E. Ayers, S.K. Ghandhi, and L.J. Schowalter: Crystallographic tilting of heteroepitaxial layers. *J. Cryst. Growth* **113,** 430 (1991).
7. J.D. Budai, W. Yang, N. Tamura, J. Chung, J.Z. Tischler, B.C. Larson, G.E. Ice, C. Park, and D.P. Norton: X-ray microdiffraction study of growth modes and crystallographic tilts in oxide films on metal substrates. *Nat. Mater.* **2,** 487 (2003).
8. C. Cantoni, A. Goyal, U. Schoop, X. Li, M.W. Rupich, C. Thieme, A.A. Gapud, T. Kodenkandath, T. Aytug, M. Paranthaman, K. Kim, J.D. Budai, and D.K. Christen: Investigation of TiN seed layers for RABiTS architectures with a single-crystal-like out-of-plane texture. *IEEE Trans. Appl. Supercond.* **15,** 2981 (2005).
9. G. Brauer and K.A. Gingerich: Oxides of cerium—V. High-temperature x-ray diffraction examination of cerium oxide. *J. Inorg. Nucl. Chem.* **16,** 87 (1960).
10. G. Brauer, K.A. Gingerich, and U. Holtschmidt: Oxides of cerium—IV. Oxygen dissociation pressure in the cerium oxide system. *J. Inorg. Nucl. Chem.* **16,** 77 (1960).
11. F. Jollet, C. Noguera, M. Gautier, N. Thromat, and J. Duraud: Influence of oxygen vacancies on the electronic structure of yttrium oxide. *J. Am. Ceram. Soc.* **74,** 358 (1991).
12. J. Duraud, F. Jollet, N. Thromat, M. Gautier, P. Maire, and C. le Gressus: Nonstoichiometry in pure and Zr-doped yttria ceramics: An EXAFS and XPS study. *J. Am. Ceram. Soc.* **73,** 2467 (1990).
13. G. Fantozzi, G. Orange, K. Liang, M. Gautier, P. Maire, and C. le Gressus: Effect of nonstoichiometry on fracture toughness and hardness of yttrium oxide. *J. Am. Ceram. Soc.* **72,** 1562 (1989).
14. A. Travlos, N. Boukos, G. Apostolopoulos, A. Dimoulas, and C. Giannakopoulos: EELS study of oxygen superstructure in epitaxial Y_2O_3 layers. *Mater. Sci. Eng., B* **109,** 52 (2004).
15. A. Dimoulas, A. Travlos, G. Vellianitis, N. Boukos, and K. Argyropoulos: Direct heteroepitaxy of crystalline Y_2O_3 on Si (001) for high-k gate dielectric applications. *J. Appl. Phys.* **90,** 4224 (2001).
16. E.D. Specht, A. Goyal, D.F. Lee, F.A. List, D.M. Kroeger, M. Paranthaman, R.K. Williams, and D.K. Christen: Cube-textured nickel substrates for high-temperature superconductors. *Supercond. Sci. Technol.* **11,** 945 (1998).
17. C. Cantoni, D.K. Christen, R. Feenstra, D.P. Norton, A. Goyal, G.W. Ownby, and D.M. Zehner: Reflection high-energy electron diffraction studies of epitaxial oxide seed-layer growth on rolling-assisted biaxially textured substrate Ni(001): The role of surface structure and chemistry. *Appl. Phys. Lett.* **79,** 3077 (2001).
18. C. Cantoni, D.K. Christen, L. Heatherly, M.M. Kowalewski, F.A. List, A. Goyal, G.W. Ownby, D.M. Zehner, B.W. Kang, and D.M. Kroeger: Quantification and control of the sulfur c (2×2) superstructure on {100}<100> Ni for optimization of YSZ, CeO_2 and $SrTiO_3$ seed layers texture. *J. Mater. Res.* **17,** 2549 (2002).